

Spontaneous Saccadic Target Selection in Gray-Scale Scenes is Based on a Structural Analysis

C. Rasche

Institut für Psychologie
Justus-Liebig Universität
Otto-Behagel-Str 10, F1
D-35394 Giessen, Germany

+ 49 (0) 641 99 26 106 (phone)
+ 49 (0) 641 99 26 119 (fax)
rasche15@gmail.com
www.allpsych.uni-giessen.de/rasche

B. Tatler

School of Psychology
The University of Dundee
Dundee
DD1 4HN, Scot, UK

Abstract

Spontaneous fixations onto shapes are driven by a structural analysis (e.g. Richard and Kaufman 1969; Melcher and Kowler, 1999). But is such analysis also carried out during free viewing of real-world scenes? Here, we analyze how fixation locations in such scenes are related to their region using their symmetric axes as a reference. Each fixation location is set into relation to its nearest symmetric axis segment by a latitude and longitude measure. Analyzing the distributions for these measures we find that there exist fixation biases for L features and parallel contours, indicating that saccadic target selection during free viewing is guided by a structural analysis.

Introduction

There exist two principal approaches to the study of spontaneous saccadic target selection. One approach has studied where exactly saccades on simple shapes and structures (e.g. Richard and Kaufmann, 1969; Melcher and Kowler 1999) and it has yielded insight into the possible mechanisms of shape analysis for target selection. The other approach has focused on an analysis of fixation locations in gray-scale scenes and has attempted to characterize target selection in terms of a mere statistical or simple-feature analysis, yet completely ignoring the former approach (e.g. Reinagel and Zador 1999; Itti and Koch 2001; Tatler et al, 2005). But there has been no effort to extend the findings of the former approach to the analysis of fixations made in real-world scenes. In this study we attempt to step into that direction.

Richard and Kaufmann found that when subjects' are asked to move their focus on a simple shape, that they place their gaze at varying but preferred locations: for close shapes (triangle, circle, rectangle) saccades in or around their center; for intersecting lines (hair cross, gap between two aligned straight lines) they directly on the intersection; for a rectangular L feature they toward the corner. Kaufman and Richard (1969) explain these observations by proposing that those preferred locations can be associated with the symmetric axes obtained from Blum's symmetric-axis transform (1967). Melcher and Kowler analyzed this ing behavior with much more scrutiny. They explored three possible types of saccadic targets: the center-of-gravity (COG), the center-of-area (COA) and the symmetric axis. For a given shape, the COG was taken as the average location of all contour pixels, the COA as the center-of-mass of the shape when it is filled with points of uniform density. Subjects were instructed to move their focus from a fixation cross to the shape without particular time pressure. The shape extended ca. 2 degrees and was around 4 degrees eccentric (from the hair cross). Under these rigid conditions, a subject's focus s closest to the COA. This clearly showed that the process of saccadic target selection relies on a thorough structural analysis.

But does this structural analysis also occur when complex scenes are viewed? The line-drawing studies by Noton and Stark evidence that this may be so (1971). Originally, the authors sought evidence for the presence of a fixed, temporal order in fixation locations. Even though this seems not to be the case in this strong form, the data clearly show that subjects tend to fixate intersecting contours as well as regions: for instance for the non-sense shape (left column of their figure on page 42) some saccades ed near the intersection of the joint between a straight line and a circle – for several subjects; for the right column (head with hand at chin), subjects tend to fixate the pattern depicting the fingers of the hand. These examples allow concluding that even a complex structural analysis occurs for the purpose of saccadic target selection during free viewing.

Does this structural analysis also take place in gray-scale images in which a structure is typically expressed across different levels of the fine/coarse scale? Just by looking at the fixation locations in figure 1, one can observe that subjects sometimes look into regions, for instance at the brick texture of the wall. Even though those saccades maybe guided by the texture, their exact ing position could be influenced by region processing taking place at a coarser level, for which the texture is not existent. To find out, we carry out a systematic analysis for the different levels of the fine/coarse scale. For each level of the fine/coarse scale, the symmetric axes for its contour image are evolved and the relative distances of the fixation locations to the axes are determined. Other shape-processing mechanisms (COA, COG) are difficult to apply, as they operate cleanly only on segmented shapes, which a typical gray-scale image does not offer.

To describe the specific relation between a fixation point and its region, a fixation point is set into relation to its nearest symmetric-axis (sym-axis) segment using two measures, the *latitude* (ϕ) and the *longitude* (λ). This is firstly exemplified on the sym-axis for two parallel lines (figure 1a). The latitude describes the distance between the fixation point and the sym-axis segment and is given as the relative location on a scale ranging from the contour side ('cnt') to the sym-axis side ('sax'; see axis below). The longitude describes the relative location of the fixation point along the sym-axis segment and is given on a scale ranging from one end to the other ('end' to 'end'). Figure 1b shows the two measures for a fixation point placed in an L feature. Figure 1c shows the example for a fixation point placed in a rectangle; the fixation point is closest to the sym-axis segment representing the two long parallel lines – the determined latitude and longitude measures essentially correspond to the parallel case shown in figure 1a.

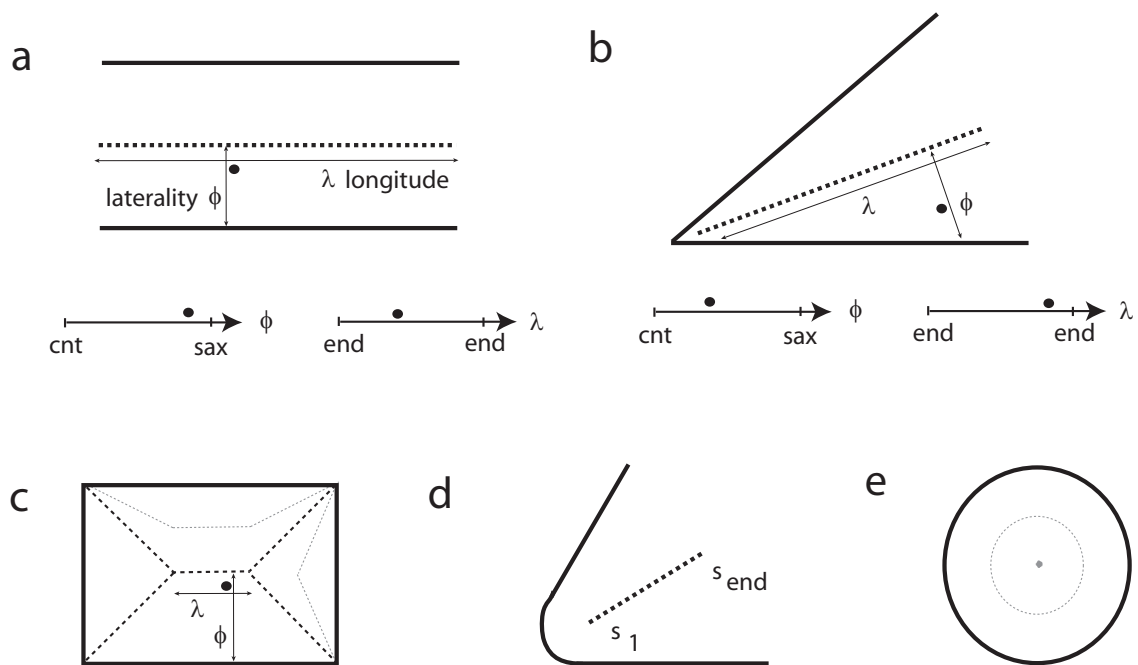


Figure 1. Symmetric axes (sym-axes) and distance measures latitude (ϕ) and longitude (λ) for a given fixation point. **a.** Example of the measures for two parallel lines: sym-axis is black dashed; fixation point is a small circle. The two scales below show how the relative location of the fixation point are denoted in later figures (figures 3 to 5). **b.** Example L feature. **c.** Example rectangle. The shown fixation point is closest to the sym-axis segment representing the parallel lines (thin dashed gray lines denote the half distance between contour and sym-axis segment). **d.** Determining the sym-axis angle exploiting the initial distance (s_1) and end distance (s_{end}) taken from the propagation field. **e.** Example circle: the sym-axis is just a point. The thin dashed circle describes the half distance between contour and symmetric axis.

Methods

The symmetric-axis transform. There exist different kinds of implementations of the symmetric-axis transform. For instance Feldman and Singh provide an implementation which aims at a precise description of complex areas (2006), but which operates only on closed shapes. But in this study, the SAT is rather used as in Blum’s original proposal (1967, 1973), namely as a method to determine the region outlined by any structure. Our implementation is best demonstrated by looking at its output. The first step is to let the contours of CF propagate until all contours have collided. This temporal evolvment is held as scalar values as a 2D map, the propagation field PF , and is shown in the upper right of figure 2: bright areas denote the center of regions (high PF value) and the sym-axes can already been recognized as ‘veins’ running through the regions. The propagation field can be regarded as a scape, in which contours run like rivers through the valley bottom and crests of the hills correspond to the symmetric axes. No plateaus are existent in the propagation field. For a model generating the propagation field PF we refer to Rasche (2007). It is only pointed out that the temporal evolvment of the PF is strongly quantized (aliased) due to the required nature of the analog propagation process (traveling wave). This can be observed for the largest region in figure 2, where the brightness values increase in a pyramidal fashion (near-rectangular structure at top-center).

To extract the sym-axes, the propagation field is convolved with a high-pass filter emphasizing the veins (ridges of the scape). Subsequent thresholding and thinning results in the sym-axis as shown in figure 2 lower left. The sym-axes for an entire image are also expressed as SF , a sparse image with values equal the PF value at the points delineating the sym-axes. In the present implementation, the high-pass filter is a DOG with standard deviations of 0.833 and 1.5. It can be seen that the implementation is largely robust to contour fragmentation (figure 2). Little contour gaps are sealed during the propagation process and leave only a small sym-axis.

Sym-axes segments. The sym-axes field is then segregated into its constituent sym-axis segments, SF_{seg} , by simply detecting intersections (shown as triangles in figure 2, lower right). For instance, the sym-axes of a rectangle are segregated into 5 segments (figure 2c) of which 4 segments describes the corresponding corners and one segment describes the central segment expressing the parallel, longer lines. Exploiting the scalar values of the sym-axes field SF , the geometry of a segment’s area is described in relatively great detail and allows to select specific geometries, such as L features (two intersecting lines), parallel lines, minimum spatial width and so on. The SF_{seg} values are normalized by the arc length l_{seg} of the segment as it lies in the image plane. The sequence of normalized symmetric points for a segment is now called $s(l_{seg})$. Because many segments show increasing distance values, corresponding to an L feature or converging lines, an initial and an end symmetric distance is defined, s_l and s_{end} , respectively (see figure 1d). For the

sym-axes segment of two exactly parallel lines $s_l = s_{end}$. From these two values the approximate angle of the L feature can be calculated. The minimum width of the sym-axis segment is defined as $2 * \min(s)$, and equals $2 * s_l$ in case of an L feature.

Latitude and Longitude. The latitude ϕ can practically be determined exploiting the propagation field. For a given fixation i_{fix} and its nearest segment SF_{seg} , the relative distance ϕ to the nearest point k_{near} on the sym-axis is

taken: $\phi = PF(i_{fix}) / SF_{seg}(k_{near})$. If the fixation lies exactly on a contour pixel then

$PF(i_{fix})$ is 0, if the fixation lies exactly on a sym-axis pixel, then $PF(i_{fix}) = SF_{seg}(k_{near})$.

Hence ϕ ranges from 0 to 1. The longitude can be determined without notable issues and is also defined as ranging from 0 to 1.

Images & fixation data. The dataset by Tatler et al (2005) was employed. It consists of the recording of 22 subjects viewing 120 images for the first 5 seconds each. Each high-resolution image subtended 30 degrees horizontally and 22 degrees vertically. A total of ca. 40000 fixations were collected. To obtain a random set of fixations for a given image, the set of fixations of all observer for a different image are taken. For each image I_1 , a pyramid of five down-sampled images was generated, taking half the resolution for successive higher levels (I_2, \dots, I_5). To obtain the (binary) contour image CF , each level of the pyramid was processed with the Canny algorithm at the finest scale ($\sigma=1$). Later, the term scale refers solely to the pyramid and not the sigma value of the Canny algorithm.

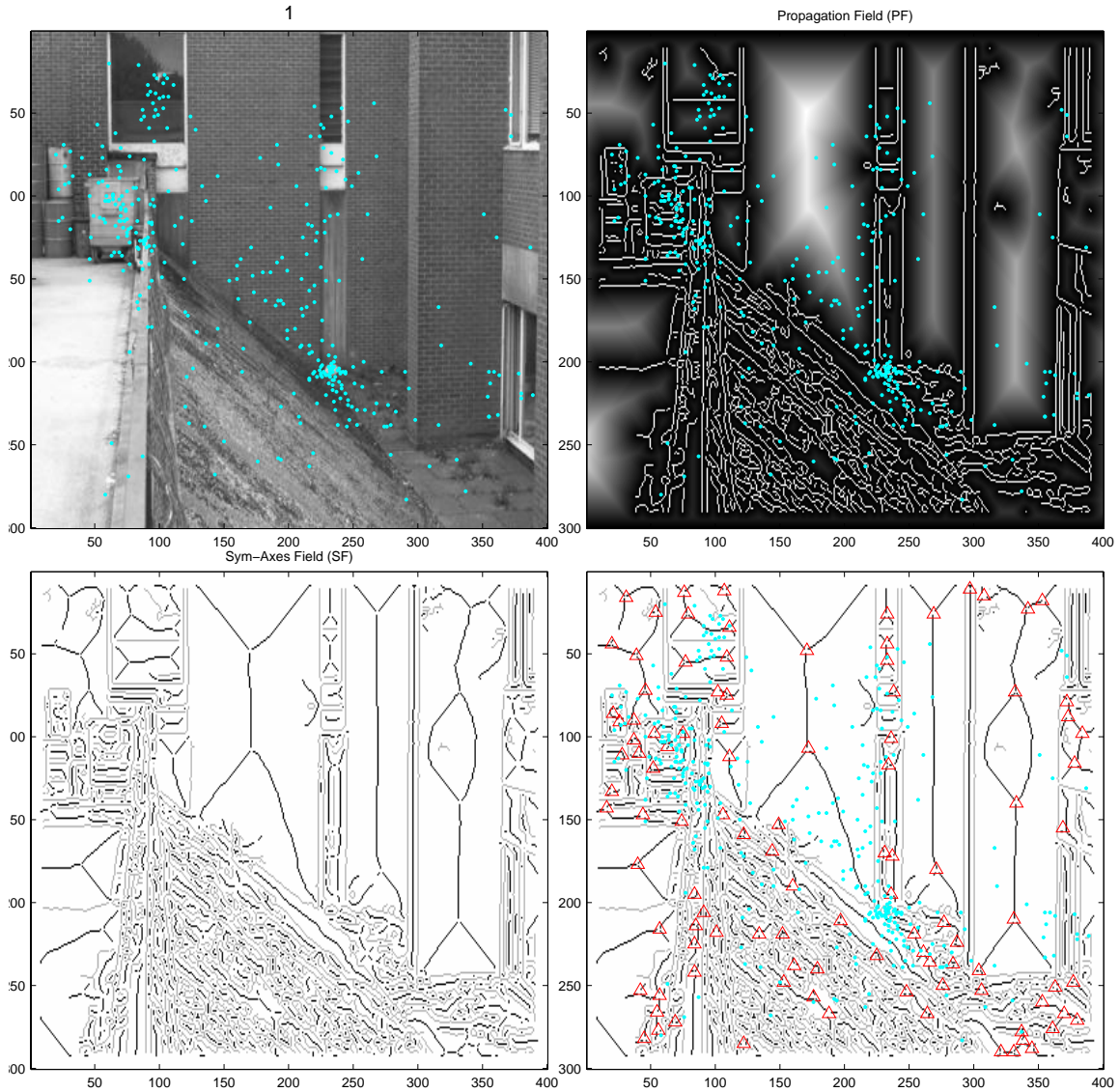


Figure 2. Example of a symmetric-axis transformation of a contour image (cyan dots denote fixation locations for 22 subjects for the first 5 seconds of viewing; image taken at 3rd scale (I_3). **Upper right:** Propagation field with symmetric axes already visible as veins in the regions (contours in white; regions are bright). **Lower left:** Contours (gray) and symmetric axes (black), respectively. **Lower right:** Intersections of sym-axes segments marked with red triangles.

Results

A first step is to look at the latitude for large sym-axes in general, that is sym-axes with a minimum width of 3.0 degrees of visual angle. This is not a very discerned way of looking at the issue of saccadic target selection, as no specific geometry has been selected, but it is part of a systematic analysis to understand the distributions of more

specific features. Figure 3 shows the latitude histogram for fixations and random selections (green and red, respectively). The x-axis of a distribution corresponds to the chosen distance definition, a value of 0 denotes the side of the contour, and a value of 1 denotes the side of the nearest sym-axis segment (see also figure 1). The random distribution decreases and is not a constant distribution due to the scape nature of the propagation field. Exemplified on the case of a circle (see figure 1e), the points with distances larger than a value of 0.5 form a concentric circle (around the symmetric point), which is smaller than the points from distances larger than a value of 0.5 (toward the contour). Thus, random selection of points from a circle will result in a distribution with a bias toward the contour side. The human distribution starts slightly higher and decreases faster and then stays below the random distribution. Blue shows the positive difference between the two distributions. This indicates that fixations tend to lie closer to the contour than to their nearest sym-axis segment. The distributions look similar for different scales but change systematically in their amplitude and their degree of decay. This is captured by fitting exponential functions to each distribution. The lower left two plots in figure 3 show how the amplitude and decay rate change across scale: for coarser scales the amplitude value decreases and the decay becomes shallower. To compare the human distribution against the random one, the human parameter values were divided by the random ones (lower right plot, figure 3). For increasing scale the human amplitude and decay rate increases slightly, indicating that on a coarser scale, fixations are placed even closer to the contour. 20 bins were used for these histograms as the data are relatively ‘analog’, but when small sym-axes are included, the distributions become quantized due to the quantization effect of evolving the propagation field (see supplementary material figure 1 for all distributions [all, small and large sym-axes]). Later histograms use 10 bins.

A large number of sym-axes segments represent L features. Figure 4 shows latitude distributions for L features of varying angle for different scales. Because angles of a specific size (e.g. 90 degrees) are rare, we determine these distributions for 3 bandwidths covering small, medium and large angles of 0 to 17, 18 to 45 and 45 to 135 degrees, respectively. Larger angles are not generated by the symmetric-axis transform. Sharp-cornered L features, as the one depicted in figure 1b, are also rare. For that reason, we included also sym-axes representing round-cornered L features (figure 1d), which are essentially a mixture between a circle and a sharp-cornered L feature: the sym-axis starts with some delay – as if a circle or oval is to be evolved – but then gradually evolves like a sharp-cornered L feature. The conditions for L feature selection were therefore, a) an initial symmetric-distance value of $s_I < 0.2$, b) a minimum length of the sym-axis segment, which was larger than the minimum symmetric distance ($l_{seg} > s_I$). The distributions now show the effects of quantization (as opposed to figure 3) due to the inclusion of small

areas. For small angles, there is little systematicity across scales: there is only a tendency to place the fixation toward the contour. For medium angles, there human distribution exceeds the random one at $\varphi=0.2$. For large angles, it also exceeds at that value but also at $\varphi=0.6$ for scales 4 and 5. None of these distributions are statistically different (t-test), but the systematic pattern across scale indicates that these are substantial biases. The last row shows the sum of all distributions and the difference of the summed distributions. In summary, for L features fixations tended to be placed a bit away from the contour, in particular for medium and large angles. It appears that for increasing angle size, fixations are placed further away from the contour and more into the open area.

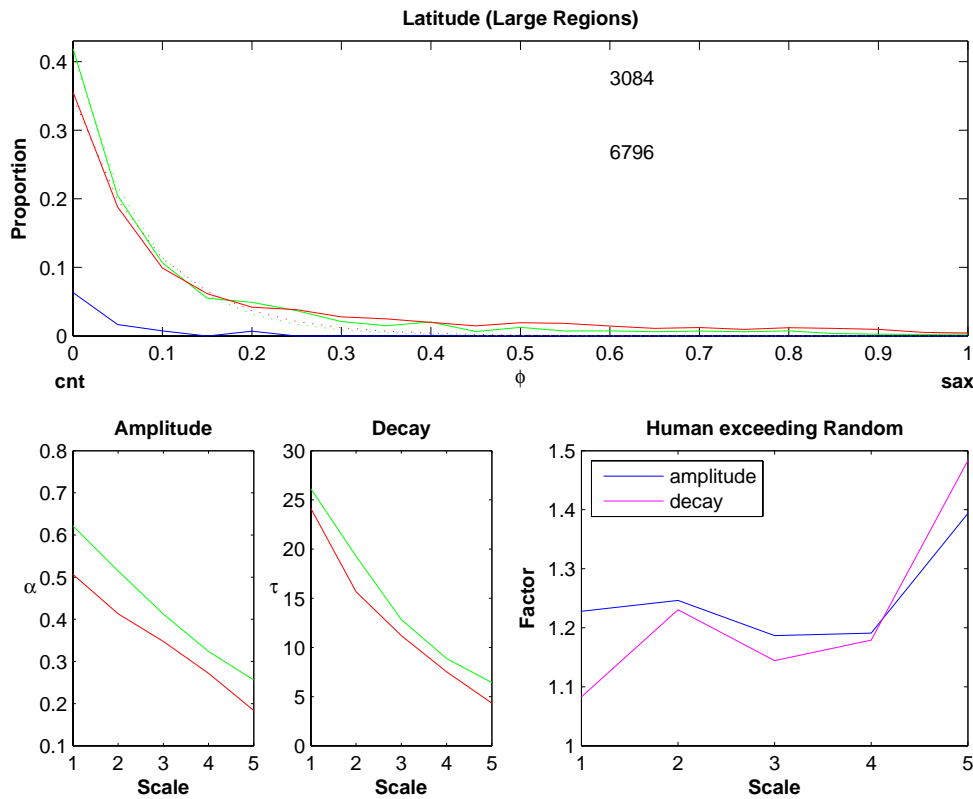


Figure 3. Latitude for large sym-axes. **Top plot:** Latitude histogram for scale 3. Last row contains sum across all scales. X-axis: Latitude ranges from 0 (contour) to 1 (sym-ax). Green: human fixations; red: random fixations; blue: positive difference of human distribution minus random distribution. The two numbers denote the number of human and random fixations for each selection (upper and lower respectively). The dotted curves are exponential fits ($\alpha e^{(-\tau\phi)}$). **Lower left two plots:** amplitude (α) and decay rate (τ) of the fits for the 5 different scales (I_1, \dots, I_5). **Lower right plot:** Factor by which the human distribution exceeds the random distribution ($\alpha_{\text{rnd}}/\alpha_{\text{hum}}$ and $\tau_{\text{rnd}}/\tau_{\text{hum}}$).

We now turn toward the longitude measure, which is characterized in figures 5 and 6. It is determined only for ‘elongated’ sym-axes segments, whose arc length is at least as long as the minimal spatial width ($l_{\text{seg}} \geq s_l$). For shorter arc lengths the longitude

measure is of limited explanatory power. The left column in figure 5 displays the distributions for those elongated segments (labeled ‘all’). The human distribution exceeds the random distribution at two approximate locations, once around a value of $\lambda=0.15$ and once around $\lambda=0.7$. In the 2nd column, the distribution for two parallel lines (straight or curved) are displayed, which were selected by choosing a maximum angle of 3 degrees. The human distribution exceeds the random one at similar locations as for the general case, but more clearly. In addition, a larger elevation for the (positive) difference distribution in the center ($\lambda=0.5$) is visible. These parallel-structure fixations were then split into two groups according to their degree of latitude, either nearer to the contour ($\varphi<0.5$; 3rd column) or nearer to the sym-axis segment ($\varphi\geq 0.5$; 4th column). Near-contour distributions showed difference peaks toward either half of the elongated, parallel structure, whereas near-sym-axis distributions also had a bias for fixations around the center. Latitude histograms for parallel contours did not show any particular differences (see supplementary material figure 4), neither could we find any particular differences in longitude histograms for vertical or horizontal parallel contours – they both were similar to the distributions as in figure 5.

Figure 6 contains the longitude measures for the L features with same angular bandwidths as before. For small angles the human longitude distribution is larger at multiple locations, but notably around the center for scale 4 and 5. The summed distribution (last row) however shows a small bias toward the open half of the L feature. For medium angles the positive-difference distribution shifts toward the left. For large angles, the positive-difference distribution is clearly on the side of the corner. Summarized, there seems to exist a progression from placing the focus to the open side for small-angled L features, to placing it to toward the apex side for large-angled L features.

A number of other distributions were analyzed. Saccadic amplitudes were partitioned into small and large sizes (<3 degrees and >6 degree respectively) and the corresponding, ensuing fixations used for creating latitude distributions, but those did not seem to differ from the ones shown so far (see supplementary material figure 2). Saccades were also partitioned into early and late saccades (<750ms and >3500ms since stimulus onset), but the latitude distributions did not show particular differences either (see supplementary material figure 2). We also generated latitude distributions for the intersection points of the sym-axis (triangles in figure 2, lower right graph). This represents a more direct measure of whether fixations are drawn to the center of a region. The latitude distributions for large intersections with a minimum width of 3.0 degrees yielded distributions very similar to the latitude distributions for sym-axes segments (figure 3 top graph). For small intersections, there appeared to be a shift away from the contour and toward the intersection point for for higher scales, especially scales 4 and 5 (see supplementary material figure 3).

Discussion

There exist clear biases on where the visual system places its focus on a structure. But because these appear as tendencies only in our analysis, it may suggest that during free viewing of natural scenes saccadic target selection relies only limitedly on a structural analysis. This is not necessarily so. One difficulty is that gray-scale images are ‘noisy’. For instance speckled noise can generate sym-axes which do not necessarily correspond to human perception, e.g. the small contour segment at $x \approx 320$ and $y \approx 100$ has caused the generation of two sym-axes (figure 2). In this sense the use of gray-scale images is not ideal and it may be useful to this analysis for recordings made in line-drawings. However, structural information is also represented across different scales, which again justifies our approach using gray-scale images. Another difficulty is that it is almost impossible to determine the exact point of saccadic target selection, namely for two reasons, the measurement error and the saccadic amplitude variability: the measurement error of the eye-tracker is approximately 0.5 degrees, a general lower limit of eye-gaze recordings (cite book Tatler); saccadic amplitudes toward targets are slightly inaccurate, with a typical mean saccadic-amplitude error of ca. 8-10% (Becker, 1972; Henson, 1997). Melcher and Kowler have compensated for that variability in some of their analysis by measuring the error for individual subjects using a circle (1999). It may therefore be the case that saccadic target selection is exact, but that the ballistic saccade system is not capable of generating a high-precision trajectory. Another complicating issue is the circumstance that saccades do not necessarily need to be accurate in ing, because structure can be recognized translation invariant to some extent (e.g. in the parafovea; Rayner 1998; Kirchner and Thorpe 2006). Thus, it suffices for a (primary) saccade – with the purpose of identifying a piece of structure - to in its approximate neighborhood. This constitutes in some way an uncertainty principle of anchoring a fixation location to its exact selected saccadic target position. When high precision is necessary, as for instance for localizing objects during manipulation, a corrective (secondary) saccade takes place – or even a sequence of small amplitude saccades. For these reasons we interpret the findings as evidence that an elaborate and possibly high-precision, structural analysis takes place during free viewing, which is used for determining the ing point of the next saccade.

For L features of small angle, the longitude measure evidenced that fixations tended to be placed in the open side (figure 6, 1st column). The corresponding latitude measurement suggests that the fixations are placed just next to the contour (figure 4, 1st column). This fixation behavior is almost identical to what has been measured by Richards and Kaufman for isolated, small-angled L features (1969; Figure 1, see figure 5 in supplementary material). For increasing angles the fixations shifted toward the corner and

for large angles some fixations can even be placed in the apex (figure 6, 3rd column). That fixations are sometimes exactly placed in the apex was also observed for some subjects (Richards and Kaufman, 1969), but also in studies in which the task was to count the number of corners of a polygon (Guez et al. 1994). It may well be that one or the other L feature is part of a vertex feature, but vertex features are rare in gray-scale scenes and no attempt was made to select them.

For parallel structures, fixations tended to be placed either toward one half of the elongated structure accompanied by a bias toward the contour side, or are placed toward the middle of the structure with a bias toward the center (sym-axes) of the enclosed area (figure 5, 3rd and 4th column). No differences could be found between the fixations made on vertical and horizontal contours.

A number of other biases of fixation locations were searched for as for instance differences for small and large saccadic amplitudes or early and late saccades, but no substantial differences could be found. Other studies have found such differences, e.g. Tatler et al. 2006. The lack of any such differences in our study is not a final verdict. Maybe such differences exist for various types of geometries and exhaustive testing may uncover further differences. For that purpose, the method of generating the sym-axes also needs to be refined. The present implementation represents a first but not final solution to the issue.

Can this be used to make better fixation predictions as for instance a discrimination between a fixated patch and a randomly selected patch? Possibly. There are a number of studies performing such a prediction which can be divided into two types. One type pursues a statistical search, such as the original study by Reinagel and Zador (1999), or the support-vector machine approach by Kienzle et al (2006). The other type performs a preprocessing of the image akin to the early visual system using simple features, such as orientation, blob and color (Itti and Koch, 2001; Tatler et al 2005). However, such a free-viewing prediction will always be limited for two reasons. One is the just-mentioned uncertainty principle of anchoring the fixation point, which therefore does not allow for an exact comparison between different observers or between observer and model. The other reason is the individuality of the human observer, an issue which contributes even more to the difficulty of making comparisons.

But other points of criticism can be raised. For instance, in Kienzle's study (2006) the goal was to find possible saccadic targets using the classification method of support-vector machines. One major finding was that the ideal fixation patch – computed from the space set up by the actual optimal fixation patches - is a center-surround structure akin to the receptive field of the early visual pathway. But that is not very specific finding with regard to the precise saccadic target mechanism. It is rather their figure 4b –

showing the most effective of the set of all actual optimal fixation patches – that the focused loci are structures such as vertices, corners, parallel contours and so on. The studies seeking a simulation of the early visual pathway (Itti and Koch, 2001; Tatler et al 2005) are often motivated by the results of experimental search studies describing parallel processing (pop-out) of visual structure using simple feature displays (e.g. Treisman and Gormican, 1982). But those experimental studies also show that more structural dimensions may contribute to saliency. Taking Treisman and Gormican’s study as an example (1982), it seems that curvature, contour length and angle between contours are other dimensions of structural analysis (figures 5, 10 and 11 respectively – all parallel phenomena). Even grouping operations, such as the presence of a small shape inside a large one, are part of parallel processing (figure 12). All these studies allow for a moderate prediction given a set of fixation and random patches, but they can also not pinpoint toward specific mechanisms of saccadic target selection. Other studies, purely computationally motivated, have achieved equally good prediction performance (Marsman et al, 2007).

Our analysis so far has rather supported the findings by the Kaufman and Richards’ studies (1969) who favored to associate their fixations locations with the symmetric axis transform. However, they did not provide a detailed model of how exactly the fixation points are determined using the sym-axes. Other studies have found that fixations closer to the COG for line-drawing shapes or cluster of dots (Melcher and Kowler, 1999), or are determined by the contrast when counting corners of a polygon (Guez et al, 1994). One reason for the different findings is that they all use different shapes and task instructions. For instance in Melcher and Kowler’s study, the subject is asked to carry out a primary saccade toward a complex structure. In such situations there may indeed be a preference to place the focus on the COA. This mechanism may well exist during free-viewing as well, but we have not yet attempted to find such a preference. One difficulty is to extract the exact area of a shape in a gray-scale image – which is more complex than just an L feature or parallel structure -, because they are often enclosed only by fragmented contours. A caveat to consider is that there may be multiple mechanisms at work which are given varying priority depending on the context of the structure and task.

A question which is rarely asked is what is the purpose of those specific fixation locations? Because structure can be recognized translation independent, one may wonder why those preferred fixation locations exist at all. They may exist for varying purposes such as accurate spatial measurement to determine the precise relation between contours, objects or scene parts. Viewing experiments with specific task instructions may provide answers to that question.

Another question is how those points are computed accurately. It is only Guez et al (1994) who give a precise model for the corner-counting task. But the computation of a COA is not as easy to achieve as it seems – in particular in not-segmented scenes. It is actually the sym-axes themselves which can deliver such a point, as they outline the area by their distance values. Thus, the sym-axes themselves may not be the saccadic target, but they maybe used for computing such targets.

Acknowledgements

CR is supported by the Gaze-based Communication Project (contract no. IST-C-033816, European Commission within the Information Society Technologies). BT is supported...

References

- [1]Becker, W. (1972). The control of eye movements in the saccadic system. *Bibliotheca Ophthalmologica*, 82, 233-43.
- [2]Blum H., (1973) "Biological shape and visual science .1." *Journal Of Theoretical Biology*, vol. 38, no. 2, pp. 205–287, 1973.
- [3]Blum H., (1967) "A new model of global brain function." *Perspect Biol Med.*,10(3): 381-408
- [4]Feldman J and Singh M. (2006). Bayesian estimation of the shape skeleton. *Proc Natl Acad Sci U S A*. 21;103(47): 18014-9.
- [5]Guez JE, Marchal P, Le Gargasson JF, Grall Y, O'Regan JK. (1994). Eye fixations near corners: evidence for a centre of gravity calculation based on contrast, rather than luminance or curvature. *Vision Res*. Jun;34(12):1625-35.
- [6]Henson, DB. (1979). Investigation into corrective saccadic eye movements for refixation amplitudes of 10 degrees and below. *Vision Res*. 19(1):57-61.
- [7]Itti, L. and Koch, C. (2001). Computational modelling of visual attention. *Nature Reviews Neuroscience*, 2(3):194--203.
- [8]Kaufman, L. & Richards, W. (1969). Spontaneous fixation tendencies for visual forms. *Perception & Psychophysics*, 5 (2), 85-88.
- [9]Kirchner, H. & Thorpe, S.J. (2006). Ultra-rapid object detection with saccadic eye movements: Visual processing speed revisited. *Vision Research*, 46, 1762-1776.
- [10]Melcher, D. & Kowler, E. (1999). Shapes, surfaces and saccades. *Vision Research*, 39, 2929-2946.
- [11]Noton,, D. & Stark, L. (1971a). Scanpaths in saccadic eye movements while viewing and recognizing patterns. *Vision Research*, 11, 929-942.
- [12]Treisman, A. & Gormican, S. (1988). Feature analysis in early vision: Evidence from search asymmetries. *Psychological Review*, 95 (1), 15-48.
- [13]Rasche C., "Neuromorphic excitable maps for visual processing," *IEEE Transactions on Neural Networks*, vol. 18, no. 2, pp. 520–529, 2007.
- [14]Rasche C. and Koch C. (2002). Recognizing the Gist of a Visual Scene: Possible Perceptual and Neural Mechanisms. *Neurocomputing*. Vol 44-46. p 979-984.
- [15]Rayner, K. (1998). Eye movements in reading and information processing. 20 years of research. *Psychological Bulletin*, 124, 372-422.
- [16]Reinagel, P. & Zador, A. M. (1999). Natural Scene statistics at the centre of gaze. *Network: Computation in Neural Systems*, 10, 341-350.
- [17]Richards, W., and Kaufman, L. (1969). 'Center of gravitiy' tendencies for fixations and flow patterns. *Perception and Psychophysics*, 5, 81-84.
- [18]Kaufman, L. & Richards, W. (1969). Spontaneous fixation tendencies for visual forms. *Perception & Psychophysics*, 5 (2), 85-88.

- [19] Tatler, B. J., Baddeley, R. J. & Vincent, B. T. (2006). The long and the short of it: Spatial statistics at fixation vary with saccade amplitude and task. *Vision Research*, 46, 1857-1862.
- [20] Tatler, B. W., Baddeley, R. J. & Gilchrist, I. D. (2005). Visual correlates of fixation selection: Effects of scale and time. *Vision Research*, 45, 643-659.
- [21] Thorpe, S.J., Fize, D. & Marlot, C. (1996). Speed of processing in the human visual system. *Nature*, 381, 520-522.
- [22] Marsman JBC, Yanulevskaya V, Cornelissen FW, et al. (2007). Spatial statistics of natural images predict gaze direction. *Perception*. Vol: 36, 35-36.

Latitude L-Feature

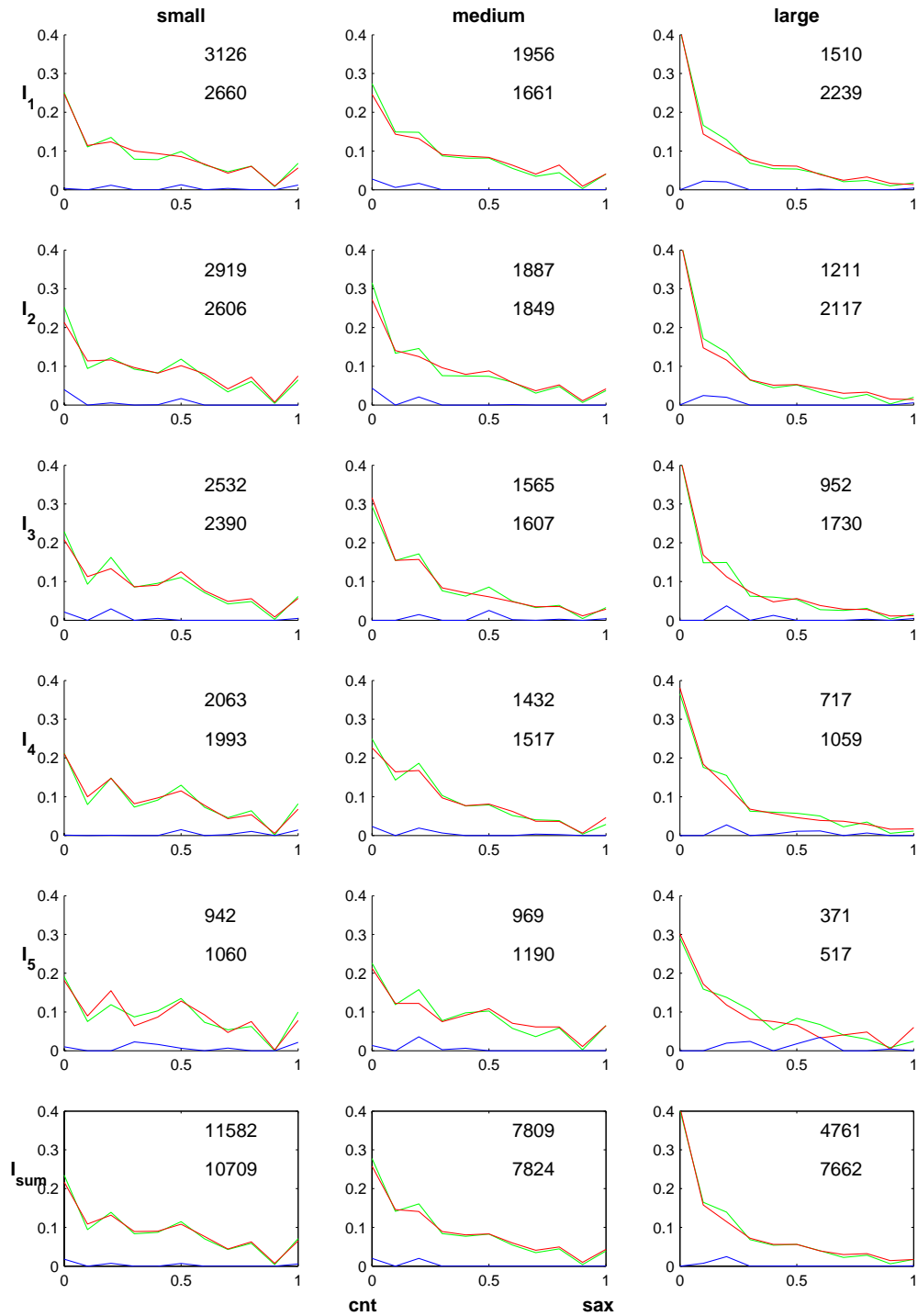


Figure 4. Latitude histograms for L features for three angle bandwidths (column wise: small [0-17], medium [18-45] and large [46-135] degrees) for different scales (row wise: I_1 to I_5 , bottom row contains sum across scales I_{sum}). X-axis: Latitude ranges from 0 (contour) to 1 (sym-axis segment).

Longitude Various Geometries

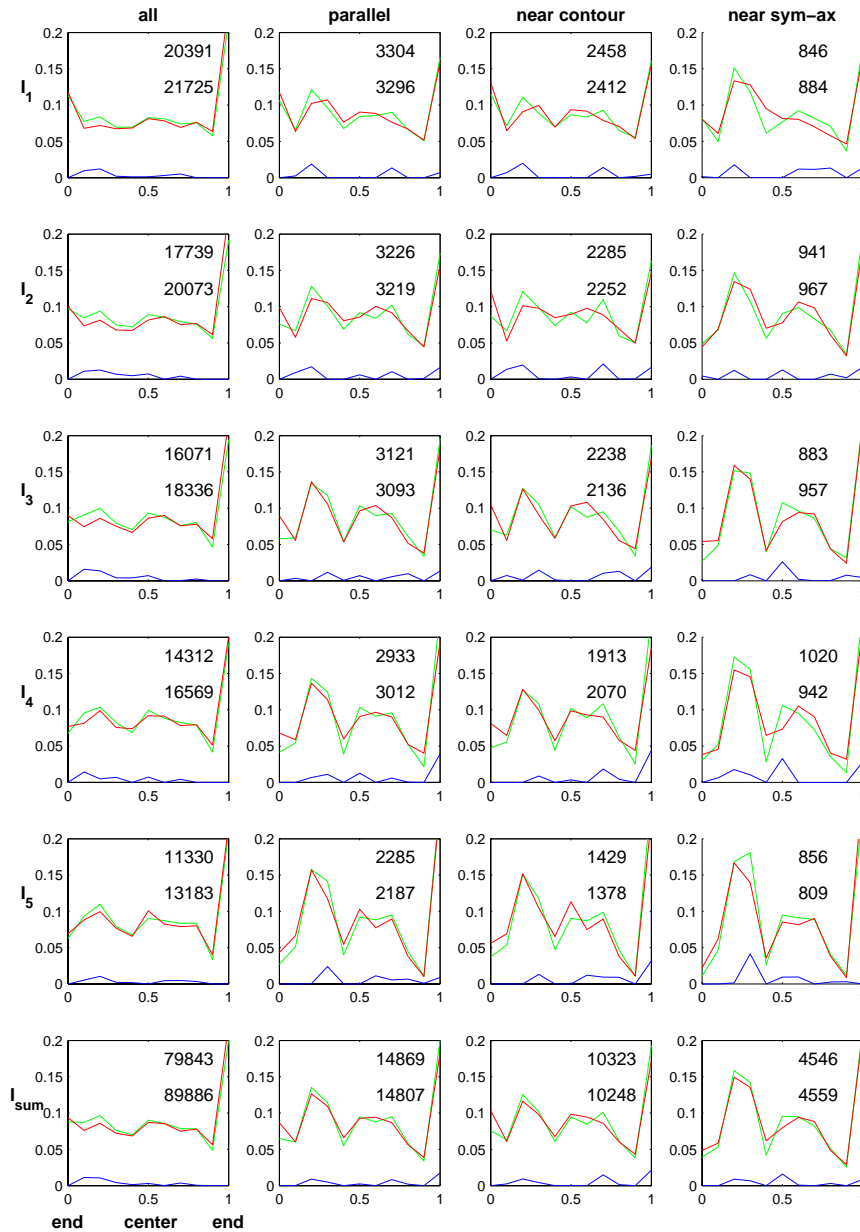


Figure 5. Longitude histograms for different scales and some specified geometries. X-axis: Longitude ranges from 0 to 1 (one end to the other end), with 0.5 denoting the center (half-way). Green: human fixations; red: random fixations; blue: positive difference of human distribution minus random distribution. Left column: Longitude for all fixations near elongated sym-axes. 2nd column: Longitude for parallel contours. 3rd column: Longitude for fixations near contour. 4th column: Longitude for fixations near sym-axes. The two numbers denote the number of human and random fixations for each selection.

Longitude L-Feature

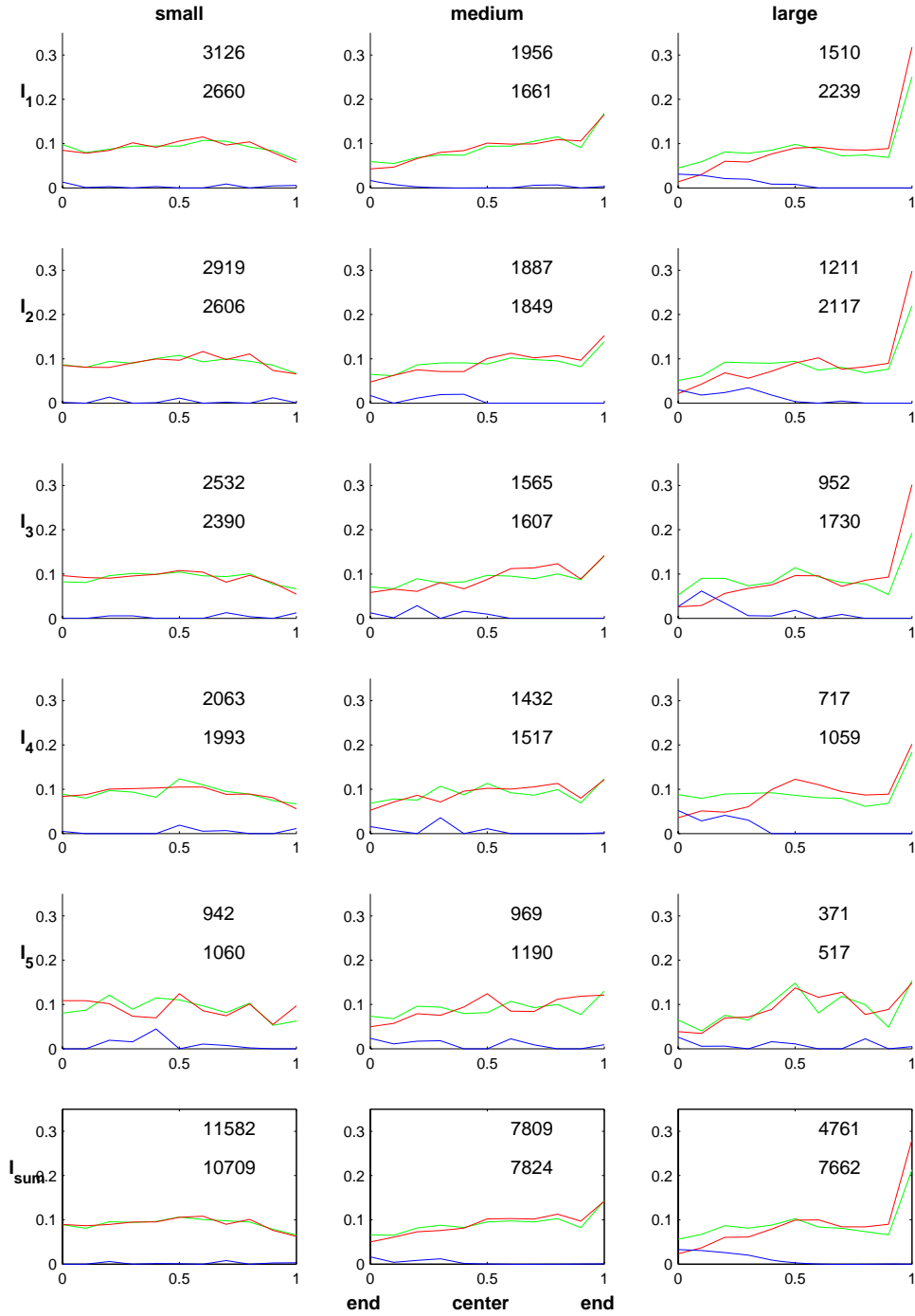


Figure 6. Longitude histogram for L features of varying angle and across scales (same angle bandwidths as in previous figures).